

Optical field characteristics of nanofocusing by conical metal-coated dielectric probe

Kazuo Tanaka,^{1,*} Kiyofumi Katayama,² and Masahiro Tanaka¹

¹Department of Electronics and Computer Engineering, Gifu University, Yanagido 1-1, Gifu City, 501-1193, Japan

²Faculty of Administration and Informatics, University of Hamamatsu, Hamamatsu City, 431-2102, Japan

*tanakazu@gifu-u.ac.jp

Abstract: Nanofocusing of surface plasmon polariton by a conical metal-coated dielectric probe was investigated numerically using the three dimensional volume integral equation. The basic characteristics of the nanofocused optical fields generated by this probe were investigated in detail. The intensity distribution near the probe tip was found to be very sensitive to the shape of the probe tip. Enhanced local fields interfere near the tip for certain probe tip shapes.

©2011 Optical Society of America

OCIS codes: (230.7370) Waveguides; (240.6680) Surface plasmons; (260.2110) Electromagnetic optics.

References and links

1. J. Takahara, S. Yamagishi, H. Taki, A. Morimoto, and T. Kobayashi, "Guiding of a one-dimensional optical beam with nanometer diameter," *Opt. Lett.* **22**(7), 475–477 (1997).
2. S. A. Maier, M. L. Brongersma, P. G. Kik, S. Meltzer, A. A. G. Requicha, and H. A. Atwater, "Plasmonics - A route to nanoscale optical devices," *Adv. Mater. (Deerfield Beach Fla.)* **13**(19), 1501–1505 (2001).
3. K. Tanaka and M. Tanaka, "Simulations of nanometric optical circuits based on surface plasmon polariton gap waveguide," *Appl. Phys. Lett.* **82**(8), 1158–1160 (2003).
4. W. L. Barnes, A. Dereux, and T. W. Ebbesen, "Surface plasmon subwavelength optics," *Nature* **424**(6950), 824–830 (2003).
5. S. I. Bozhevolnyi, V. S. Volkov, E. Devaux, J. Y. Laluet, and T. W. Ebbesen, "Channel plasmon subwavelength waveguide components including interferometers and ring resonators," *Nature* **440**(7083), 508–511 (2006).
6. V. M. Shalaev and S. Kawata ed., *Nanophotonics with Surface Plasmons* (Elsevier Science Ltd., 2007).
7. M. Ohtsu, K. Kobayashi, T. Kawazoe, T. Yatsui, and M. Naruse, *Principles of Nanophotonics* (Chapman and Hall, 2008).
8. A. J. Babadjanyan, N. L. Margaryan, and K. V. Nerkararyan, "Superfocusing of surface polaritons in the conical structure," *J. Appl. Phys.* **87**(8), 3785 (2000).
9. M. I. Stockman, "Nanofocusing of optical energy in tapered plasmonic waveguides," *Phys. Rev. Lett.* **93**(13), 137404 (2004).
10. M. W. Vogel, D. K. Gramotnev, and K. Dmitri, "Adiabatic nano-focusing of plasmons by metallic tapered rods in the presence of dissipation," *Phys. Lett. A* **363**(5-6), 507–511 (2007).
11. F. De Angelis, G. Das, P. Candeloro, M. Patrini, M. Galli, A. Bek, M. Lazzarino, I. Maksymov, C. Liberale, L. C. Andreani, and E. Di Fabrizio, "Nanoscale chemical mapping using three-dimensional adiabatic compression of surface plasmon polaritons," *Nat. Nanotechnol.* **5**(1), 67–72 (2010).
12. K. Kurihara, A. Otomo, A. Syouji, J. Takahara, K. Suzuki, and S. Yokoyama, "Superfocusing modes of surface plasmon polaritons in conical geometry based on the quasi-separation of variables approach," *J. Phys. A: Math. Theor.* **40**(41), 12479–12503 (2007).
13. K. Kurihara, K. Yamamoto, J. Takahara, and A. Otomo, "Superfocusing modes of surface plasmon polaritons in a wedge-shaped geometry obtained by quasi-separation of variables," *J. Phys. A: Math. Theor.* **41**(29), 295401 (2008).
14. A. V. Goncharenko, M. M. Dvoynenko, H.-C. Chang, and J.-K. Wang, H.-C. Chang, and J.-K. Wang, "Electric field enhancement by a nanometer-scaled conical metal tip in the context of scattering-type near-field optical microscopy," *Appl. Phys. Lett.* **88**(10), 104101 (2006).
15. W. Chen and Q. Zhan, "Numerical study of an apertureless near field scanning optical microscope probe under radial polarization illumination," *Opt. Express* **15**(7), 4106–4111 (2007).
16. K. Tanaka, G. W. Burr, T. Grosjean, T. Maletzky, and U. C. Fischer, "Superfocussing in a metal-coated tetrahedral tip by dimensional reduction of surface-to-edge plasmon modes," *Appl. Phys. B* **93**(1), 946–2171 (2008).
17. D. K. Gramotnev, M. W. Vogel, and M. I. Stockman, "Optimized nonadiabatic nanofocusing of plasmons by tapered metal rod," *J. Appl. Phys.* **104**(3), 034311 (2008).
18. T. J. Antosiewicz, P. Wróbel, and T. Szoplik, "Nanofocusing of radially polarized light with dielectric-metal-dielectric probe," *Opt. Express* **17**(11), 9191–9196 (2009).

19. F. I. Baida and A. Belkhir, "Superfocusing and Light Confinement by Surface Plasmon Excitation Through Radially Polarized Beam," *Plasmonics* **4**(1), 51–59 (2009).
 20. W. Ding, S. R. Andrews, and S. A. Maier, "Internal excitation and superfocusing of surface plasmon polaritons on a silver-coated optical fiber tip," *Phys. Rev. A* **75**(6), 063822 (2007).
 21. A. Downes, D. Salter, and A. Elfick, "Simulations of atomic resolution tip-enhanced optical microscopy," *Opt. Express* **14**(23), 11324–11329 (2006).
 22. N. A. Issa and R. Guckenberger, "Optical nanofocusing on tapered metallic waveguides," *Plasmonics* **2**(1), 31–37 (2007).
 23. N. A. Issa and R. Guckenberger, "Fluorescence near metal tips: The roles of energy transfer and surface plasmon polaritons," *Opt. Express* **15**(19), 12131–12144 (2007).
 24. D. K. Gramotnev, M. W. Vogel, and M. I. Stockman, "Optimized nonadiabatic nanofocusing of plasmons by tapered metal rod," *J. Appl. Phys.* **104**(3), 034311 (2008).
 25. K. Tanaka, K. Katayama, and M. Tanaka, "Nanofocusing of surface plasmon polaritons by a pyramidal structure on an aperture," *Opt. Express* **18**(2), 787–798 (2010).
 26. L. W. Davis and G. Patsakos, "TM and TE electromagnetic beams in free space," *Opt. Lett.* **6**(1), 22–23 (1981).
 27. L. W. Davis, "Theory of electromagnetic beams," *Phys. Rev. A* **19**(3), 1177–1179 (1979).
-

1. Introduction

There has been great interest in theoretical and experimental studies of nanometric integrated optical circuits that employ surface plasmon polaritons (SPPs) [1–7]. A basic problem in this area is how to couple incident light into metallic nanostructures since conventional optics cannot focus a laser beam into a region that is much smaller than about half the wavelength of the light due to the diffraction limit of light.

One promising technique is superfocusing or nanofocusing by SPPs [8–13]. It is possible to focus a radially polarized optical SPP mode along a cylindrical metal surface by reducing the cylinder cross section. A practical way to achieve this is to use tapered or conical metal structures [8–19]. Such structures are also used as plasmonic optical probes for near-field scanning optical microscopes (NSOMs) [20, 21] and consequently they have been intensively investigated.

In the early analysis of such structures, analytical methods based on the adiabatic approximation were used [8–11]. A more accurate analytical method based on the perturbation method has been reported [12, 13]. Since the rigorous solution is unknown, analytical treatments inevitably have to employ some form of approximation. To overcome the limitations of analytical methods, various numerical methods have been applied to the problem, including finite-difference time-domain (FDTD) method [14–19], the finite integration technique (FIT) [20], the finite element method (FEM) [21–24] and the volume integral equation method (VIE) [16,25].

Using the above analytical and numerical techniques, most studies have mainly considered how to generate a strongly focused and strongly enhanced optical field at a tip. The basic characteristics of the enhanced local fields that are nanofocused near the probe tip have been insufficiently investigated due to the difficulty in accurately calculating the field distribution near the tip even using the numerical techniques. For example, the spatially staggered vector components of the electric and magnetic fields about unit cells are employed in the conventional FDTD method. Thus, the boundary between the probe tip and free space is not well defined, making it difficult to investigate the relation between the enhanced field near the tip and structure of the probe tip. Since the structure is assumed to consist of tiny cubes in the VIE method, these cubes provide a clear boundary between the tip and free space, making it possible to investigate the relation between the enhanced local fields and the probe tip structure. So far, the relation between the probe tip shape and the nanofocused SPP optical fields near the probe-tip has not been investigated.

In the present study, the VIE method is used to investigate nanofocusing of SPPs by a conical metal-coated dielectric probe. In particular, the basic characteristics of the nanofocused optical fields are investigated in detail. A metal-coated conical probe is a promising structure to use when using SPP nanofocusing techniques in the practical applications [15, 18, 20]. We demonstrate that for specific probe tip shapes enhanced local fields interfere near the tip.

2. Geometry of the problem

Figure 1 shows a schematic diagram of the metal-coated conical dielectric probe on a metal screen considered in this study. The conical dielectric probe with a relative permittivity ϵ_2 is fabricated on a rectangular metal screen with dimensions $B_x \times B_y \times B_z$ in the x - y plane of the (x, y, z) coordinate system shown in Fig. 1. The conical probe has a base radius R and a height h . The side of the conical dielectric probe is coated with metal with thickness d and relative permittivity ϵ_1 . This conical probe is rotationally symmetric about its center axis. The center axis of the probe is coincident with the z -axis (see Fig. 1). The surrounding free space has a permittivity ϵ_0 .

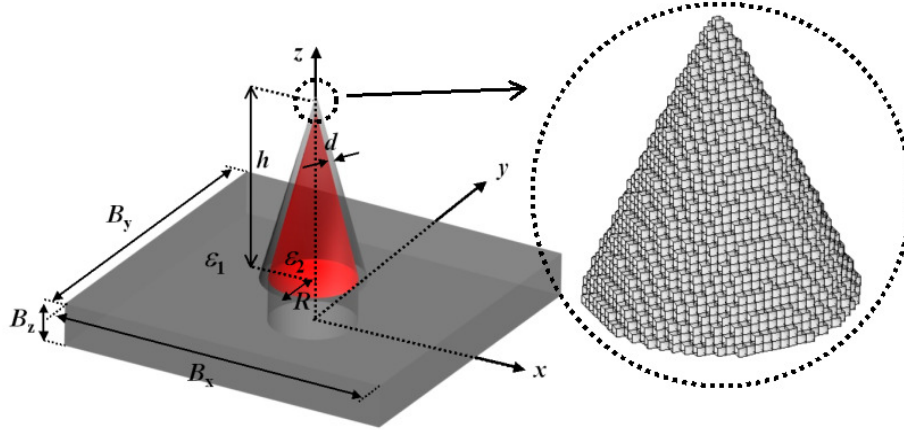


Fig. 1. Geometry of the metal-coated conical dielectric probe on a metal screen. The metal screen has dimensions $B_x \times B_y \times B_z$ and is located in the x - y plane. The conical structure has a base-radius R and a height h . The dielectric conical probe is coated with a metal whose permittivity is ϵ_2 . The metal coating has a thickness d . The metal screen contains a circular aperture of radius $R-d$. Permittivities of the surrounding free space, screen, and dielectric in the conical structure are denoted by ϵ_0 , ϵ_1 and ϵ_2 , respectively. A radially polarized Gaussian beam is normally incident on the screen from the negative z direction. The beam axis coincides with the z -axis. The whole structure is discretized into the tiny cubes of size δ , as depicted in the inset.

The screen has a circular aperture whose center is located at the center of the probe and whose radius is $R-d$ (see Fig. 1). A radially polarized Gaussian beam is normally incident on the screen from the negative z -direction below the metal screen. The beam axis lies along the z -axis. The radial and z components of the incident electric field at $z=0$ can be written as [26, 27];

$$\begin{aligned} E_r(r, 0) &= 2A(r/w) \exp[-(r/w)^2] \\ E_z(r, 0) &= -j4A[1 - (r/w)^2] / (k_0 w) \exp[-(r/w)^2], \end{aligned} \quad (1)$$

where k_0 is the wavenumber in free space, w is the spot size of the beam and $r = (x^2 + y^2)^{1/2}$. The beam amplitude is determined as $A = 1$ in this study by assuming that the incident beam has the same energy as a linearly polarized beam of unit amplitude with the same spot size. The incident beam illuminates the metal-coated conical probe through the circular aperture in the screen. A radially polarized SPP is excited on the probe surface and the optical field of the SPP is nanofocused by the decreasing cross section of the probe in the propagation direction.

We solve the scattering problem shown in Fig. 1 by the VIE method [16, 25]. We first discretize the whole structure shown in Fig. 1 using tiny cubes; i.e., we consider that the conical structure and the screen are composed of cubes with dimensions $\delta \times \delta \times \delta$. In the treatment by the VIE method, the surface of the probe is not smooth. However, since the small roughness cannot be avoided in the practical probes, the irregular surface of the probe shown in the inset of Fig. 1 is not unrealistic. We then discretize the VIE by the method of moments

(MoM) using rooftop functions as basis and testing functions in each cube. Finally, we solve the resultant system of linear equations numerically by general minimum residual method with fast Fourier transformation. In this paper, the value of δ is given by $k_0\delta = 0.05$ ($\delta = 5$ nm). The size of the cube used for the discretization of the structure is usually equal to that used in applying the MoM to the VIE. However, in this study, we mostly use cubes with a size of $\delta/2$ (2.5 nm) when applying the MoM to the VIE, whereas we discretize the structure by a cubes of size δ . This means that each cube of size δ , that makes up the whole structure, is further subdivided into eight smaller cubes of size $\delta/2$ in the numerical calculations by the MoM.

In the simulation, the wavelength is $\lambda = 633$ nm, and the complex permittivities of the metal screen and the coating metal are $\epsilon_1/\epsilon_0 = -13.8 - j1.08$ (Au) in the most cases. We assume that the screen is made of the same metal as the coating metal. The permittivity of the dielectric is $\epsilon_2/\epsilon_0 = 2.25$. The beam spot size of is $w = \lambda$ at $z = 0$. The rectangular screen has dimensions $k_0B_x = k_0B_y = 15.45$ ($B_x = B_y = 1557$ nm) and $k_0B_z = 0.95$ ($B_z = 96$ nm). The thickness d of the metal coating cannot be specified precisely because the side of the metal-coated probe is bumpy since it is composed of cubes (see inset of Fig. 1). Thus, we specify the average thickness to be $k_0d=0.27$ ($d=27.4$ nm) in this paper.

3. Optical intensity distributions of a typical metal-coated conical dielectric probe

We first consider an idealized mathematical model of a typical conical structure that has as apex angle 37 degrees and a base radius given by $k_0R = 7.07$ ($R = 712$ nm). We refer this structure as probe 1. We discretize it using cubes arranged in 328 layers parallel to the x - y plane (see Fig. 1). Probe 1 has a height given by $k_0h = 16.4$ ($h = 1652$ nm). Figure 2(a) shows the arrangement of the cubes in the top 14 layers. We characterize the shape of the discretized probe tip by the numbers of cubes in each layer. Probe 1 has **137-113-97-89-69-61-45-37-29-21-13-9-5-1** cubes in the top 14 layers (from bottom to top) (see Fig. 2(a)). Bold letters indicate that the part composed of these numbers of cubes does not change in the various probes considered hereafter. Figure 2(b) shows the structure when each cube is subdivided into eight cubes of size $\delta/2$ in for applying the MoM to the VIE. Note that the shapes shown in Figs. 2(a) and 2(b) are not rotationally symmetric about the probe axis due to discretization of the structure by the cubes. However, they are symmetric with respect to the x - z and y - z planes.

To confirm the validity of the numerical results, we first solve the problem using cubes of size δ when discretizing the probe structure for the VIE by the MoM. Figures 3(a) and 3(b) respectively show the distributions of the x - and the z -components of the electric field in the x - z plane (i.e., $\text{Im}[E_x(x, 0, z)]$ and $\text{Im}[E_z(x, 0, z)]$) for probe 1. We then solve the problem using cubes of size $k_0\delta = 0.025$ ($\delta/2 = 2.5$ nm) in the discretization for the VIE; in other words, we use the structure shown in Fig. 2(b) instead of that in Fig. 2(a). Figures 3(c) and 3(d) show the

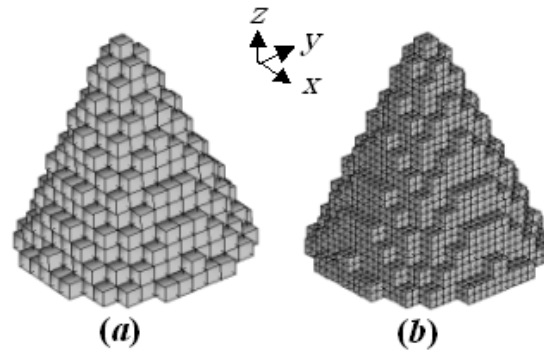


Fig. 2. Arrangement of cubes that makes probe 1. The cubes in only top 14 layers are shown. There is a total 328 layers ($k_0h = 16.4$), which are parallel to the x - y plane. (a) The probe structure is discretized by cubes of size $k_0\delta = 0.05$ ($h = 5$ nm). (b) Each cube shown in (a) is divided into eight smaller cubes of size $\delta/2$ ($= 2.5$ nm) when applying the MoM to the VIE.

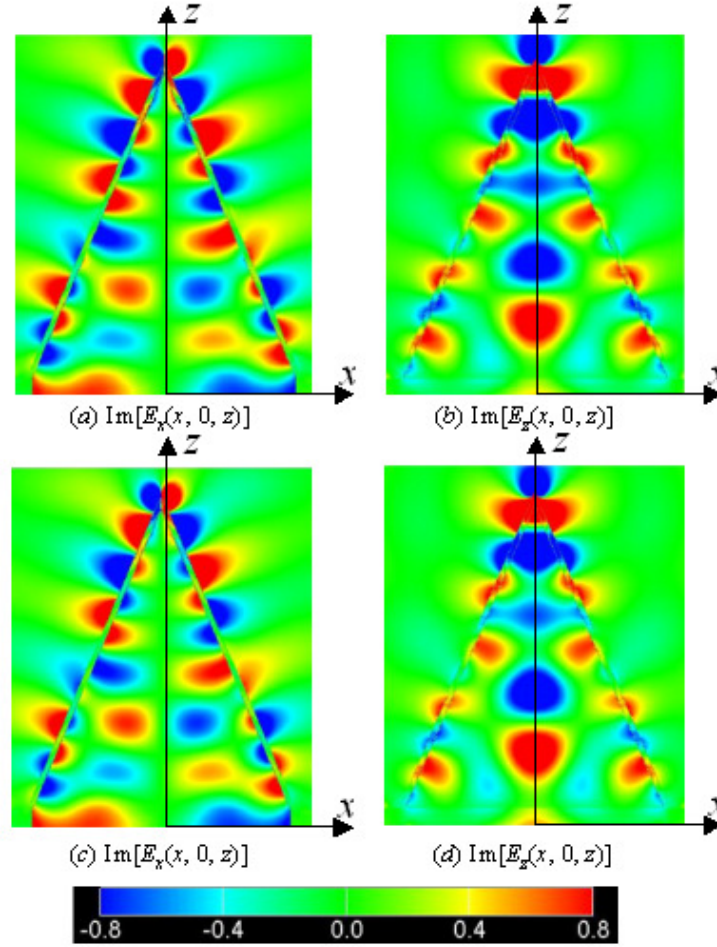


Fig. 3. Distributions of electric field components in the x - z plane for probe 1. $\text{Im}[E_x(x, 0, z)]$ is shown in (a) and (c), and $\text{Im}[E_z(x, 0, z)]$ is shown in (b) and (d). The results of (a) and (b) were obtained using discrete cubes with δ (5 nm) and (c) and (d) were obtained using discrete cube with $\delta/2$ when applying MoM. The whole structure is composed of tiny cubes of size δ . The metal coating is Au ($\epsilon_2/\epsilon_0 = -13.8 - j1.08$).

results for the x - and z -components of the electric field in the x - z plane, respectively. Figures 3(a) and 3(b) are very similar to those in Figs. 3(c) and 3(d), which implies that the numerical results are largely independent of the size of the cubes used in the MoM. This confirms the validity of the calculation results of this study. The results shown in Fig. 3 indicate that, SPP excited along the metal coatings is focused on the probe tip and that the main component of the focused electric fields is the z -component on the tip. In all the following numerical calculations, a size $\delta/2$ (2.5 nm) is used in the discretization of the VIE by the MoM.

We next investigate the basic characteristics of the enhanced local field near the probe-tip. Figure 4(a) shows a typical distribution of the optical intensity $|\mathbf{E}(x, 0, z)|^2$ in the x - z plane near the probe tip for probe 1. The enhanced local optical field has a maximum intensity of $\sim 6.0 \times 10^4$ on the upper surface of the top cube in free space. Figure 4(b) shows the vector characteristics of the local field $\text{Im}[\mathbf{E}(x, 0, z)]$ on the x - z plane for probe 1. It reveals that the enhanced local field mainly consists of radial components near the tip.

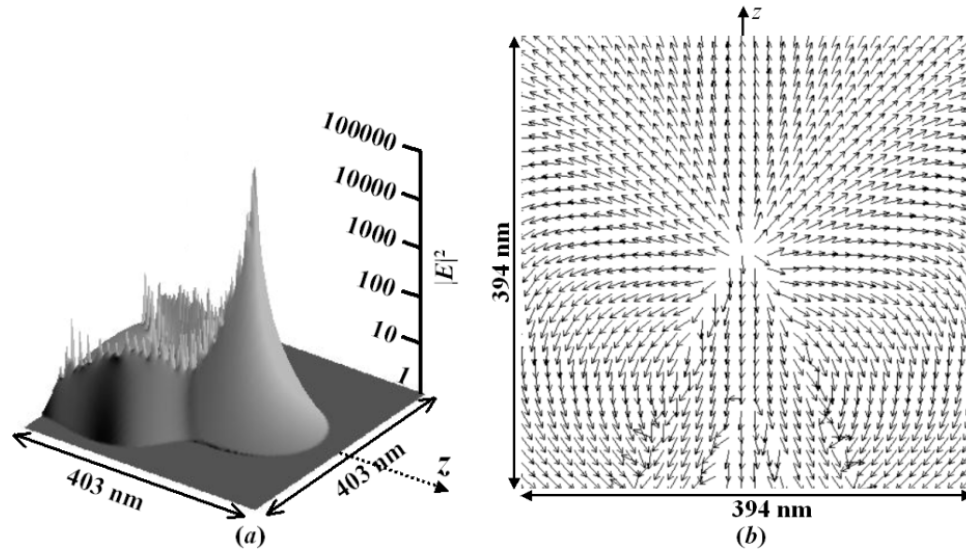


Fig. 4. (a) Optical intensity $|E(x, 0, z)|^2$ distributions in the x - z plane for probe 1. (b) Vector characteristics of the electric field $\text{Im}[E(x, 0, z)]$ in the x - z plane for probe 1. The metal coating is Au ($\epsilon_2/\epsilon_0 = -13.8 - j1.08$).

4. Dependence of optical intensity on distance from probe tip

The enhanced local optical field has been reported to be sensitive to the curvature of the probe tip [11, 24]. Probe 1 is the most suitable for modeling a simple cone structure whose diameter varies linearly along the center axis within this study. To model a tip that has less curvature, we consider three tip shapes that have smaller tip curvature than probe 1. They were formed by removing cubes from near the tip of probe 1 (see Fig. 2). Figure 5(a), 5(b), and 5(c) show the three arrangements of cubes near the tip; we refer to these arrangements as probe 2, 3, and 4, respectively. It is difficult to calculate the curvature of tip of the probes 1-4 accurately, because of the discretized structure shown in Fig. 2 and 5. However, these probes can be made by the discretization of the curved structure whose radii of the curvature are given by 7, 9, 11 and 21 nm for probes 1-4, respectively.

Using the same notation used to characterize probe 1, probe 2 has **137-113-97-89-69-61-45-37-29-21-13-9-5** cubes in 13 layers from bottom to top (Fig. 5(a)). Probe 2 is shorter than probe 1 by only δ ($k_0h = 16.35$ ($h = 1647$ nm)). Similarly, probe 3 has **137-113-97-89-69-61-45-37-29-21-13-9** cubes in 12 layers from bottom to top (Fig. 5(b)) and it is shorter than probe 1 by 2δ , ($k_0h = 16.3$ ($h = 1642$ nm)). Probe 4 has **137-113-97-89-69-61-45-37-5** cubes in the top nine layers and it is shorter than probe 1 by 4δ ($k_0h = 16.2$ ($h = 1632$ nm)). Note that probes 1-4 (see Figs. 2 and 5) have same configurations of cubes in the eight layers from the bottom to the top. (Numbers of cubes in these eight layers are written bold letter through this paper.) This means that probes 1-4 have the same configurations of cubes in 322 layers of the total 328 layers (from the base to 322th layer). They differ in only a few layers above the 322th layer. All these probes are symmetric relative to the x - z and y - z planes.

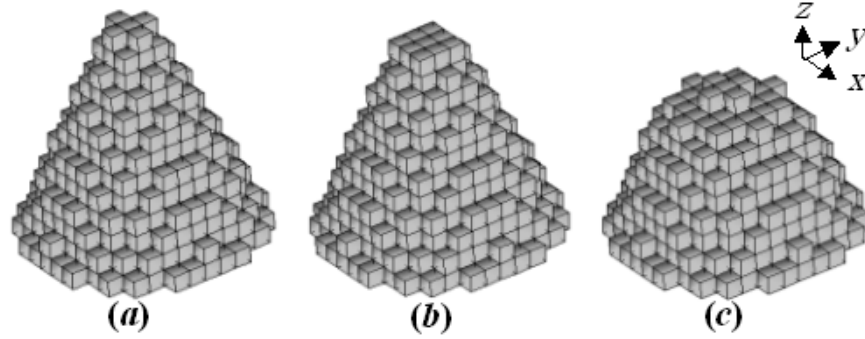


Fig. 5. Arrangements of cubes that make up the tips of (a) probe 2 ($k_0h = 16.35$), (b) probe 3 ($k_0h = 16.3$) and (c) probe 4 ($k_0h = 16.2$). These figures show the layers above 314th of the 328 horizontal layers.

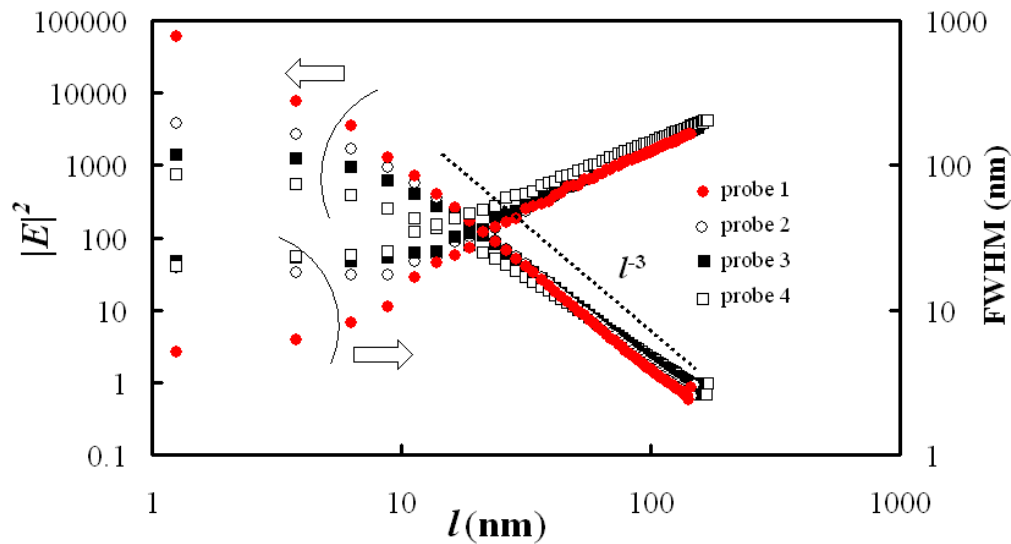


Fig. 6. Optical intensity distributions along the z -axis $|E(0, 0, l)|^2$ and FWHM (full width at half-maximum) of the intensity distributions for probes 1-4. The abscissa shows $l = z - h$, which is the distance from the upper surface of the top cube of the tip. The metal coating is Au ($\epsilon/\epsilon_0 = -13.8 - j1.08$).

Figure 6 shows the enhanced local optical intensity distributions in free space above the tip along the z -axis for probes 1-4. The abscissa shows $l = z - h$, which is the distance from the upper surface of the top cube of the tip. The dependence of the optical intensity on the distance l is important, because it determines the relation between the spot size of the nanofocused intensity and the distance l . The FWHM (full width at half-maximum) of the intensity distributions are also shown in Fig. 6. Figures 5 and 6 reveal that the maximum intensity just above the cube strongly depends on the curvature of the probe tip. The maximum intensity of probe 2 decreases from $\sim 6.0 \times 10^4$ to $\sim 3.8 \times 10^3$ on removing just the top cube whose size is 5 nm from probe 1 (see Fig. 6). The intensity decays according to l^{-3} at distances greater than 20 nm from the tip. It is well known that the optical intensity decays according to l^{-3} by semi-analytical calculations for the ideal conical structure [8, 12]. Near the probe tip, however, the intensity decays less than the dependence l^{-3} due to the finite curvature of the tip. These results agree qualitatively with the results of calculations employing analytical approximation.

5. Sharper tips

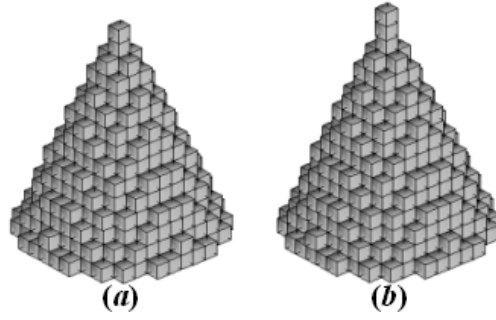


Fig. 7. Arrangement of cubes in (a) probe 5 and (b) probe 6. The figure shows (a) top 15 layers of the 329 horizontal layers and (b) top 16 layers of the 330 horizontal layers.

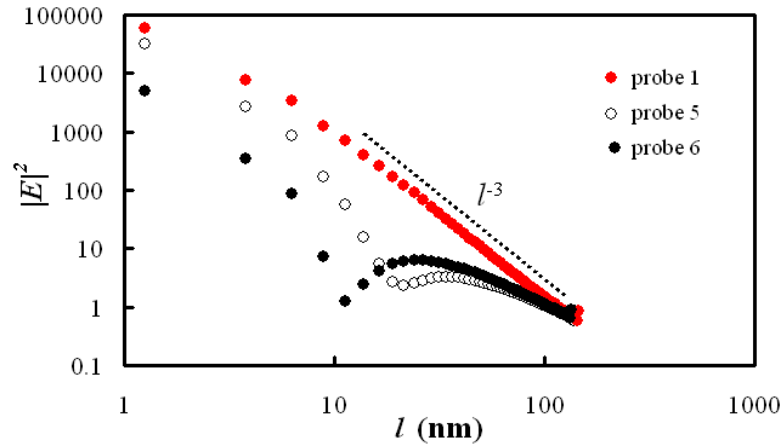


Fig. 8. Distributions of optical intensity along the z -axis $|E(0, 0, l)|^2$ for probes 4 and 5. The abscissa $l = z - h$ is the distance from the upper surface of the top cube on the tip. For reference, the solid red circles indicate the results for probe 1. The metal coating is Au ($\epsilon_2/\epsilon_0 = -13.8 - j1.08$).

We found that the nanofocused optical field is very sensitive not only to the tip curvature but also to the shape of the probe tip. To form probe tips that is sharper than probe 1, we added one and two cubes on the top of the probe 1 (see Fig. 7). We refer to the structures shown in Fig. 7(a) and 7(b) as probes 5 and 6, respectively. Probe 5 has **137-113-97-89-69-61-45-37-29-21-13-9-5-1-1** cubes in 15 layers from bottom to top ($k_0h = 16.45$ ($h=1657$ nm)) and probe 6 probe has **137-113-97-89-69-61-45-37-29-21-13-9-5-1-1-1** cubes in 16 layers ($k_0h = 16.5$ ($h = 1662$ nm)) shown from bottom to top.

We can consider that probes 5 and 6 have sharper tip structure than probe 1. Figure 8 shows the dependence of the optical intensity on the distance from the tip l along the z -axis. For reference, the results for probe 1 are indicated by the solid red circles. Probes 5 and 6 respectively have the intensities at the tip $\sim 3.1 \times 10^4$ and $\sim 4.9 \times 10^3$, which are smaller than that of probe 1. These values may be due to the large attenuation of SPP that propagates along the structure of the added cubes shown in Fig. 7. Furthermore, the intensities for probes 5 and 6 do not decrease monotonically with increasing l . Figure 9 shows the intensity distribution $|E(x, 0, z)|^2$ and the vector characteristics of the electric field in the x - z plane $\text{Im}[E(x, 0, z)]$ near the tip of probe 6.

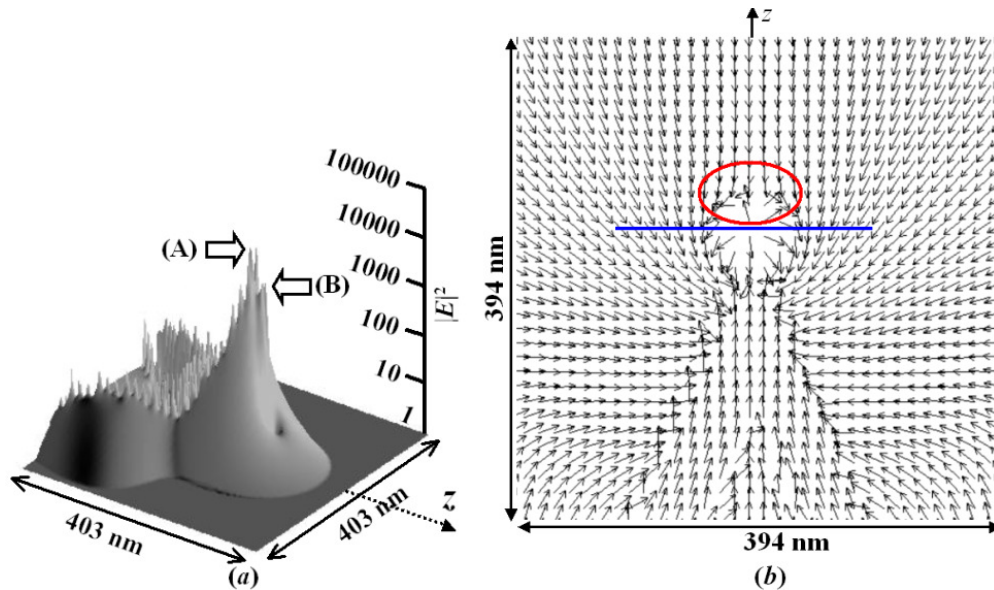


Fig. 9. (a) Optical intensity $|E(x, 0, z)|^2$ distribution in the x - z plane for probe 6. (b) Vector characteristics of the electric field $\text{Im}[E(x, 0, z)]$ in the x - z plane for probe 6. The metal coating is Au ($\epsilon_2/\epsilon_0 = -13.8 - j1.08$). The region surrounded by the red ellipse indicates the low-intensity spot and blue line indicates the boundary between the tip and the free space on the z -axis. Positions of third cube below the top cube and of the top cube are indicated by (A) and (B), respectively.

Figure 9(a) reveals that there is a low-intensity spot in the free space above the tip. In addition, it shows the intensity is not maximized above the top cube of the tip. The maximum intensity is located near the third cube below the top cube whose position is indicated by the arrow (A) and the second largest intensity occurs on the tip whose position is indicated by the arrow (B) (see Fig. 9(a)). There are two regions of enhanced local fields near the tip and each enhanced intensity has two peaks shown in Fig. 9(a). The blue line in Fig. 9(b) indicates the boundary between the tip and the free space on the z -axis. The z -components of the electric fields cancel each other in the region indicated by red circle in Fig. 9(b). From the vector characteristics of $\text{Im}[E(x, 0, z)]$, low-intensity spot is apparently caused by these two local fields interfering above the tip. This result reveals that the field distribution near the tip cannot be treated by the electrostatic approximation, because an electrostatic field cannot have a maximum or a minimum in free space. The results shown in Figs. 8 and 9 are interesting because they suggest that it may be possible to control the intensity distribution near the tip. The intensity distribution near the tip strongly depends on the tip structure.

6. Increasing the maximum optical intensities on the tip

When metal-coated probes are used in NSOM, it is preferable to maximize the optical intensity on the probe-tip. We investigated structures that give large optical fields under the simulation conditions. The tip structures shown in Fig. 7 do not increase the maximum intensity above that of probe 1. After trial and error for various tip structures, we found that the tip shape shown in the inset of Fig. 10 generates the maximum intensity that is greater than that of probe 1. This tip shape has **137-113-97-89-69-61-45-37-29-21-13-9-7-4-1** cubes in 15 layers from the bottom to top; we refer to this probe as probe 7 ($k_0h = 16.45$). Figure 10 shows the intensity distribution along the z -axis for probe 7. Probes 1 and 7 have the same configuration of cubes in the 12 layers from the bottom in Fig. 2 and inset of Fig. 10. This shape is based on the concept of smoothing the reduction in the cross section of the probe near the tip. Note that the number of cubes in the top five layers of probe 1, (i.e., 21-13-9-5-1) is changed to 21-13-9-7-4-1 in the top six layers probe 7. For reference, the solid red circles in

Fig. 10 show the results for probe 1 (Au). The maximum intensity of this probe is $\sim 1.1 \times 10^5$, which is about twice that for probe 1 (see Fig. 2). (Note that the ordinate scale of Fig. 10 is 10 times greater than that of Figs. 2 and 3.)

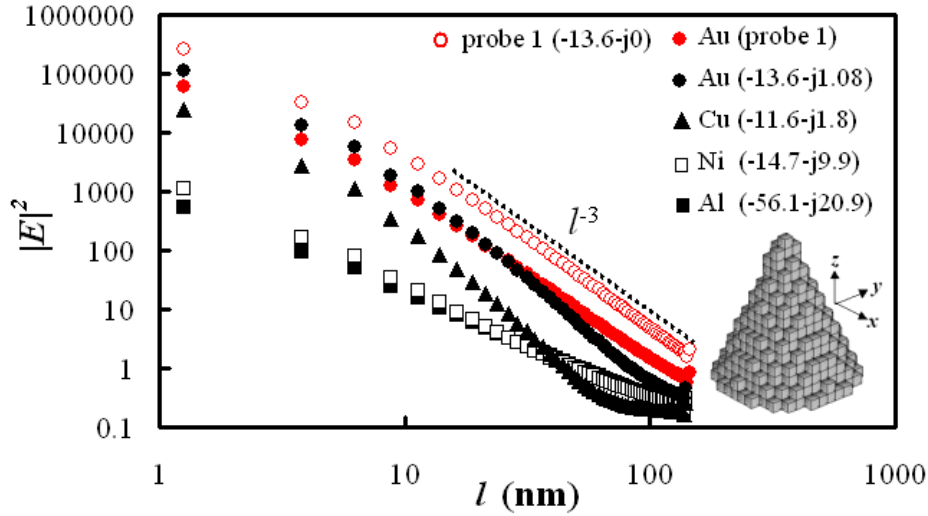


Fig. 10. Optical intensity distributions along the z -axis $|E(0, 0, l)|^2$ for probe 7 for Au and three coating metals. The Abscissa $l = z - h$ is the distance from the upper surface of the top cube on the tip. The solid red circles indicate the results for probe 1 for reference. Open red circles indicate the results under the assumption of no dissipation in probe 1 coated with Au.

Figure 10 also shows the results for three kinds of metals (Cu, Ni and Al) in addition to those of Au. The intensity dependence on distance l for probe 7 differs from l^{-3} for $l > 20$ nm. Interestingly, Cu gives a large enhanced intensity of $\sim 2.5 \times 10^4$ and rather large enhanced intensities can also be generated even by metals having large dissipations ($\sim 1.1 \times 10^3$ for Ni and $\sim 5.4 \times 10^2$ for Al).

The results indicated by the open red-circles in Fig. 10 show the results where there is no dissipation in probe 1 coated with Au. When the metal (Au) is no dissipation, the maximum intensity is $\sim 2.6 \times 10^5$ that is about 2.5 times greater than that obtained using probe 7 (see Fig. 10). The dissipation of the metal is an important factor to generate large enhanced intensity on the tip. In the results shown in Fig. 10, those for probe 1, which has no dissipation, are closest to l^{-3} for $l > 20$ nm. The dissipation of the metal and nanosized extensions on the probe tip modify the intensity distribution from l^{-3} for $l > 20$ nm.

7. Conclusions

The basic characteristics of SPP optical fields nanofocused by metal-coated conical dielectric probes have been investigated by the VIE method. The maximum enhanced field near the tip was found to be highly sensitive to the shape of the probe. The field distribution near the tip along the probe axis was modified by the tip shape and the coating metal. The findings of this study demonstrate that metal-coated conical probes must be carefully designed and fabricated. Since the developed code is fully three dimensional, it is possible to apply the code to the simulation of the image acquisition by NSOM.

Acknowledgment

This work was supported by the Grant-in-Aid for Scientific Research (C) in 2010. The calculations were performed at the Information Technology Center, Nagoya University.